Numerical simulation and characterization of speckle noise for laser Doppler vibrometer on moving platforms (LDVom)

Jin, Yang; Dollevoet, Rolf; Li, Zili

DOI
10.1016/j.optlaseng.2022.107135

Publication date
2022

Document Version
Final published version

Published in
Optics and Lasers in Engineering

Optics and Lasers in Engineering 158 (2022) 107135

Contents lists available at ScienceDirect

Optics and Lasers in Engineering

journal homepage: www.elsevier.com/locate/optlaseng

Numerical simulation and characterization of speckle noise for laser Doppler vibrometer on moving platforms (LDVom)

Yang Jin, Rolf Dollevoet, Zili Li*

Railway Engineering, Delft University of Technology, the Netherlands

ARTICLE INFO

Keywords:
Laser Doppler vibrometer
Speckle noise simulation
Surface roughness
Scanning speed

ABSTRACT

Laser Doppler Vibrometer (LDV) is extensively applied in remote and precise vibration measurements for structural monitoring. Speckle noise is a severe signal issue restricting LDV applications, mainly when an LDV scans from moving platforms. Realistic simulations and thorough characterizations of speckle noise can support the despeckle procedure. A novel approach to numerically simulate speckle noise is proposed based on the statistical properties of speckle patterns. Surface roughness and other affecting factors are thoroughly studied. The simulated distributions agree well with the literature when investigating speckle properties. Single-point and continuously scanning speckle noise are both numerically generated and experimentally acquired. Their corresponding time-series and fast Fourier spectra present good agreement. In addition, similar amplitude distributions, approximating a Gaussian distribution, are achieved. Speckle noise is different from Gaussian white noise because of the varying frequency distribution. The speckle noise grows with increasing surface roughness to a critical value. When simulating and acquiring the scanning speckle noise, the noise energy increases with the scanning speed, but the signal drop-outs decrease in intensity and density. These promising results demonstrate the simulation accuracy and can further support despeckle procedures.

1. Introduction

Laser Doppler Vibrometer (LDV) is a noncontact and nondestructive instrument for precise vibration measurement [1]. It has been extensively used in structural health monitoring (e.g., Nassif et al. [2], Sels et al. [3]) as an alternative to traditional contacting transducers. Its physical mechanism is the Doppler effect, as the target movement can cause the frequency shift of lasers. LDV is technically superior to attached sensors, acquiring vibrations remotely and continuously (e.g., measuring very long structures such as railway tracks at high speeds) and avoiding mass loading that possibly changes vibration modes [4]. In addition, the instrument has a measuring frequency over 1 GHz and a vibration velocity resolution of 1 mm/s, suitable for scenarios requiring high-frequency and high-spatial-resolution analysis. In recent decades, the LDV measurement technique has evolved from single-point measurement to pointwise measurement (scanning LDV (SLDV)) and then to the continuous scanning technique (continuous SLDV (CSLDV)) [1]. The pointwise measurement is a set of single-point measurements, and the SLDV acquires sufficient signals at each point. This technique is time-consuming. The CSLDV avoids this issue, but it requires multiple reciprocating scans (e.g., Xu et al. [4], Allen and Sracic [5], Chen et al. [6]) for modal testing and noise removal. The signal integrated by those from numerous reciprocating cycles derives the structural mode shapes. Thus, the excitation source and the structural conditions should be constant during one CSLDV measurement. An LDV on moving platforms (LDVom) [7] is proposed for one-way continuously scanning vibrating surfaces, especially for long or large structures where multiple reciprocating scans are inapplicable. The instantaneous mode shape is acquired, and either the excitation source or the structural conditions could be time-variant. However, a significant signal issue, speckle noise [1,8], becomes extremely troublesome for the LDVom since the noise effect cannot be averaged without multiple scanning.

Speckle noise is a significant issue that distorts the acquired vibration, adversely affecting signal interpretation. The noise is attributed to an optical phenomenon, namely speckle patterns, as coherent laser scattering from an optically rough surface alters the phases [9]. The laser wavelets interfere constructively or destructively and thus produce a speckle pattern with bright and dark spots. The signal outputs are phasor summations of the reflected wavelets, and thereby speckle variation, including translation and deformation of the focusing spot, results in signal fluctuations, namely speckle noise. According to the

* Corresponding author.
E-mail addresses: J.Jin-3@tudelft.nl (Y. Jin), R.P.B.J.Dollevoet@tudelft.nl (R. Dollevoet), Z.Li@tudelft.nl (Z. Li).

https://doi.org/10.1016/j.optlaseng.2022.107135
Received 21 April 2022; Accepted 3 June 2022

aforementioned scanning techniques, translation of the focusing spot occurs in two cases: (1) the structure at the focusing spot vibrates or (2) the laser continuously scans over the structure. In physical experiments, the noise amplitude reaches over 30 times the true vibration, and the signal-to-noise ratio falls below −15 db [10]. Several approaches have been developed in recent studies to reduce adverse effects, but these approaches are either poorly effective or applicability-limited. For example, Vass et al. [11] and Hosek [12] developed algorithms to eliminate signal drop-outs, but dominant speckle noise with normal amplitudes remained; Chiariotti et al. [13] and Pieczonka et al. [14] overlooked time-frequency information and only calculated the energy distribution for defect identification. These studies lack a comprehensive analysis of speckle noise, while knowing the noise characteristics can support the despeckle procedure. Others mitigated speckle noise according to the noise features, e.g., averaging signals over the cyclical measurement [15] and attaching retroreflective tapes to enhance the reflections [16]. Still, these approaches are not applicable in field measurements including railway inspection. Therefore, the realistic simulation and thorough characterization of speckle noise for better a understanding of the issue should be studied.

Noise simulation and characterization require accurate phasor calculation over the speckle patterns and proper simulation of the LDVom scanning procedure. The surface roughness dominantly affects the speckle pattern [17,18], while the scanning procedure is influenced by the focusing spot, the scanning speed and the sampling frequency. Some studies have investigated the properties of speckle patterns but lack a thorough consideration of surface roughness. Goodman [19] systematically derived the statistical properties of laser speckle patterns, but he assumed large surface roughness beyond the laser wavelength; Ohtsubo and Asakura [20] derived the intensity distribution but not the phase distribution that is significant for LDV signals; Fujii and Asakura [21] experimentally investigated the statistical distribution of the speckle intensity but not of the phase. Recently, the simulation of speckle patterns in image signals was considered. Bolter [22] adopted Gaussian white noise, which is significantly different from speckle noise. Perreault et al. [23] and Yamaguchi [24] simulated the laser intensities but ignored the phases. Martino et al. [25] adopted the K-distribution for the light intensity and uniform distribution for the light phase, but their assumption simplified the contribution of surface roughness. To the best of our knowledge, the sole study for simulating the speckle noise in LDV signals was conducted by Rothberg [26]. The speckle noise simulated in Rothberg [26], where a surface passes through a stationary laser beam with a constant speed, is similar to that in LDVom. However, the noise should be affected by surface roughness and the aforementioned factors in the LDVom scanning procedure, which have not been considered. In other research, Martin and Rothberg [9] experimentally investigated the relationship between the speckle noise and the focusing spot, while other scanning factors were not included. Therefore, the speckle-noise simulation and characterization that thoroughly consider the related factors remain to be investigated, and such a study is significant for speckle mitigation and avoidance.

In this paper, we propose a novel approach to numerically simulate the speckle noise in LDVom signals, and then characterize the noise for a better understanding of the issue. Speckle noise from the single-point vibration is also characterized since sometimes important structural nodes need constant monitoring. When analyzing the statistical properties, we consider the surface roughness thoroughly and derive the complex distribution of laser phases. Then, the speckle noise is simulated in different situations by varying the scanning speed and the surface roughness. Pure speckle noise is experimentally acquired to evaluate the simulation accuracy. The remainder of this paper is organized as follows: Section 2 derives the statistical properties and describes the simulation approach; Section 3 evaluates the simulation accuracy by comparing with the experimental results and then characterizes the speckle noise in different situations; Section 4 discusses the possible effect of the commercial demodulation system on our experimental results; and Section 5 concludes this paper.

2. Methodology

2.1. Statistical properties of speckle patterns

Since there are numerous cases of microscopic structure of the scanning surface, a better understanding of the statistical properties is necessary. The monochromatic wave equation [27] to present the field incident at (x, y, z) is

$$u(x, y, z; t) = A(x, y, z)e^{i2\pi\nu t} = \mid A(x, y, z) \mid e^{i\theta(x,y,z)}e^{i2\pi\nu t} \tag{1}$$

where, t is the transmission time, ν is the optical frequency, and $A(x, y, z)$ represents a complex phasor with the phase $\theta(x, y, z)$. Then the light intensity of the field (x, y, z) can be calculated as

$$I(x, y, z) = \lim_{T\to\infty} \frac{1}{T} \int_{-T/2}^{T/2} \mid u(x, y, z; t) \mid^2 dt = \mid A(x, y, z) \mid^2 \tag{2}$$

Considering that the complex amplitude $A(x, y, z)$ results from the summation of the laser wavelets illuminating a speckle pattern [27], the phasor amplitude can be represented by

$$A(x, y, z) = \sum_{k=1}^{n} \mid a_k \mid e^{i\phi_k} \tag{3}$$

where, $\mid a_k \mid$ and ϕ_k represent the amplitude and phase of the kth wavelet respectively, and n is the wavelet number in the speckle pattern ([20,28] provide the estimator of n). According to Eqs. (2) and (3), the wavelet amplitude $\mid a_k \mid$ equals $\frac{\sqrt{I_0}}{n}$ (I_0 is the incident light intensity). Without loss of generality, we can set the incident light intensity $I_0 = 1$. The phase ϕ_k of the reflected wavelet is proportional to the height of the irregularities of the rough surface [29–31]

$$\phi_k = \frac{4\pi}{\lambda} h_k \tag{4}$$

where h_k is the departure of the surface height from its mean value and λ is the optical wavelength. According to Eq. (4), we can derive the statistical relationships between the speckle pattern and the surface roughness

$$\begin{aligned} \mu_\phi &= \tfrac{4\pi}{\lambda} R_a \\ \sigma_\phi &= \tfrac{4\pi}{\lambda} R_q \end{aligned} \tag{5}$$

where, μ_ϕ and σ_ϕ represent the mean and standard deviation of the phases respectively, and R_a and R_q represent the mean roughness and root-mean-square roughness of the surface respectively. The phase ϕ_k becomes a random variable that is determined by the random variable h_k. According to Eq. (3), we can obtain that

$$A(x, y, z) = \frac{1}{n}\sum_{k=1}^{n} e^{i\phi_k} = \frac{1}{n}\sum_{k=1}^{n} \cos\phi_k + i\frac{1}{n}\sum_{k=1}^{n} \sin\phi_k = A_1 + iA_2 \tag{6}$$

where $A_1 = \frac{1}{n}\sum_{k=1}^{n} \cos\phi_k$ is the real component of the phasor and $A_2 = \frac{1}{n}\sum_{k=1}^{n} \sin\phi_k$ is the imaginary component. When n is a large positive integer, according to the central limit theorem (Lindeberg–Levy Theorem), we can obtain that

$$\epsilon_1 = \frac{A_1 - \mu_1}{\sigma_1/\sqrt{n}} \sim N(0, 1)\ ;\ \epsilon_2 = \frac{A_2 - \mu_2}{\sigma_2/\sqrt{n}} \sim N(0, 1) \tag{7}$$

where, μ_1 and σ_1 are the mean and standard deviation of $\cos\phi_k$, μ_2 and σ_2 are the mean and standard deviation of $\sin\phi_k$, and $N(0, 1)$ represents the standard normal distribution. On this basis, the joint probability density function of A_1 and A_2 is yielded as follows

$$f_A(A_1, A_2) = \frac{n}{2\pi\sigma_1\sigma_2} e^{-\frac{\frac{(A_1-\mu_1)^2}{\sigma_1^2} + \frac{(A_2-\mu_2)^2}{\sigma_2^2}}{2/n}} \tag{8}$$

According to Eqs. (2) and (6), the intensity I and phase φ of a speckle pattern can be expressed as

$$I = I(x,y,z) = \mid A(x,y,z) \mid^2 = A_1^2 + A_2^2$$
$$\tan\varphi = \frac{A_2}{A_1} \tag{9}$$

Considering Eq. (8), we can obtain the joint probability density function of I and φ

$$f_{I,\varphi}(I,\varphi) = \mid J \mid f_A(A_1,A_2) = \frac{n}{4\pi\sigma_1\sigma_2} e^{-\frac{\frac{(\sqrt{I}\cos\varphi-\mu_1)^2}{\sigma_1^2}+\frac{(\sqrt{I}\sin\varphi-\mu_2)^2}{\sigma_2^2}}{2/n}} \tag{10}$$

where J is the Jacobi conversion matrix. Therefore, the independent distributions of I and φ can be acquired by integrating Eq. (10) separately.

However, the integration to calculate the phase φ distribution is very troublesome. According to Eq. (9), $tan\varphi$ is a variable generated by the ratio of two independent normal variables, thus obeying the distribution derived from a known probability density function in Cedilnik et al. [32].

$$\begin{aligned} f_\varphi(\tan\varphi) &= \frac{nbd}{\sqrt{2\pi}a^3\sigma_1\sigma_2}\left[\Phi(\frac{b}{a}) - \Phi(-\frac{b}{a})\right] + \frac{1}{\pi a^3\sigma_1\sigma_2} e^{-c/2} \\ a &= \sqrt{(\tan\varphi)^2/\sigma_2^2 + 1/\sigma_1^2} \\ b &= \mu_2\tan\varphi/\sigma_2^2 + \mu_1/\sigma_1^2 \\ c &= \mu_2^2/\sigma_2^2 + \mu_1^2/\sigma_1^2 \\ d &= e^{\frac{b^2-ca^2}{2a^2}} \end{aligned} \tag{11}$$

where the function Φ is the cumulative density function of the standard Gaussian distribution. Since μ_1, μ_2, σ_1, and σ_2 are determined by μ_ϕ and σ_ϕ, the relationship between the variables I and φ and the surface roughness is established. This expression is suitable for applications with wide-range surface roughness.

In addition, the expressions of Eqs. (10) and (11) also cover those in the literature. For example, when $\sigma_1/\sqrt{n} = \sigma_2/\sqrt{n} = \sigma$ and $\mu_1 = \mu_2 = 0$, we can obtain the same expression as in Goodman [19], Rothberg [26] that the variable I follows an exponential distribution and φ follows an even distribution.

2.2. LDV speckle noise

LDV utilizes the Doppler frequency shift produced by the relative motions to detect the vibrations. The signal received by the photodetector is the summation vector of the target and reference laser beams, and the intensity scalar can be expressed as Halliwell [33]:

$$I_d = I_R + I_T + 2\sqrt{I_R I_T}\cos\left[2\pi f_R t - \frac{4\pi}{\lambda}\int v dt + (\varphi_R - \varphi_T)\right] \tag{12}$$

where, I_d is the detected intensity, I_R and φ_R are the intensity and phase of the reference beam, I_T and φ_T are the intensity and phase of the target beam respectively, f_R is the frequency of the reference beam, λ is the incident wavelength, and v is the vibration velocity of the target. Therefore, the frequency shift of the target beam is

$$f_{\text{beat}} - f_R = -\frac{2}{\lambda}v + \frac{1}{2\pi}\frac{d(\varphi_R - \varphi_T)}{dt} \tag{13}$$

Considering that the target beam illuminates P speckle patterns (each with phase φ_{Tp} and intensity I_{Tp}) and the reference beam illuminates Q speckle patterns (each with phase φ_{Rq} and intensity I_{Rq}), the resultant intensity I_{res} and phase φ_{res} are related to the summations incident on the photodetector [26]

$$I_{\text{res}} = 2\sqrt{I_R I_T} = \frac{1}{A}\left\{\left[\sum_{q=1}^{Q}\sum_{p=1}^{P} A_{pq}\sqrt{I_{Rq}I_{Tp}}\sin(\varphi_{Rq} - \varphi_{Tp})\right]^2\right.$$

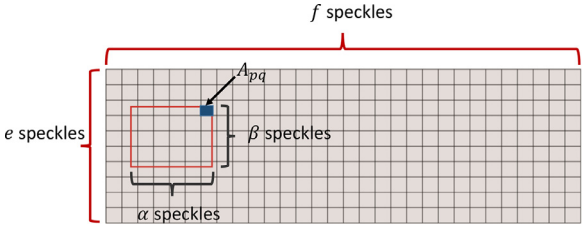

Fig. 1. Example of the divided scanning surface and the focusing spot (red rectangle).

$$\left. + \left[\sum_{q=1}^{Q}\sum_{p=1}^{P} A_{pq}\sqrt{I_{Rq}I_{Tp}}\cos(\varphi_{Rq} - \varphi_{Tp})\right]^2\right\}^{1/2} \tag{14}$$

$$\begin{aligned} \tan\varphi_{\text{res}} &= \tan(\varphi_R - \varphi_T) \\ &= \frac{\sum_{q=1}^{Q}\sum_{p=1}^{P} A_{pq}\sqrt{I_{Rq}I_{Tp}}\sin(\varphi_{Rq} - \varphi_{Tp})}{\sum_{q=1}^{Q}\sum_{p=1}^{P} A_{pq}\sqrt{I_{Rq}I_{Tp}}\cos(\varphi_{Rq} - \varphi_{Tp})} \end{aligned} \tag{15}$$

where, A_{pq} is the overlapping area of the pth target and qth reference speckle patterns. Phase variation dominantly contributes to the speckle noise even when the laser intensity is adequate. According to Eq. (13), the measured vibration V_m is the true vibration v polluted by a noisy component.

$$V_m = \frac{\lambda}{2}(f_R - f_{\text{beat}}) = v - \frac{\lambda}{4\pi}\frac{d(\varphi_{\text{res}})}{dt} = v - \frac{\lambda}{4\pi}\cdot\frac{1}{1+\tan^2(\varphi_{\text{res}})}\frac{d(\tan(\varphi_{\text{res}}))}{dt} \tag{16}$$

where $-\frac{\lambda}{4\pi}\frac{d(\varphi_{\text{res}})}{dt}$ is the so-called speckle noise or 'pseudo vibration', and the expression is rewritten with the deviation of $\tan(\varphi_{\text{res}})$. Sharp variations of the phase φ_{res} generate LDV speckle noise, adding unwanted fluctuations in the vibration signal. Therefore, the intensity and phase distributions of speckle patterns on the scanning surface affect the LDV signals. The statistical properties in Section 2.1 can be utilized for the speckle-noise simulation.

Assuming the speckle patterns are rectangular and densely distributed as in Rothberg [26], the scanning surface is divided into $e \times f$ speckle elements, as shown in Fig. 1. The size of each speckle element should ensure that sufficient laser wavelets will transmit onto a speckle and the sharp variation of the surface roughness can be characterized. Hereafter, since the true surface outliers h_k in Eq. (4) are difficult to acquire, we use the roughness parameters R_a & R_q to assign intensities and phases to the speckle elements according to Eqs. (10) and (11).

The target beam illuminates a particular area with α speckles $\times$ β speckles (the red rectangle in Fig. 1) on the scanning surface. The intensities and phases of speckles inside the focusing spot (the red rectangle) constitute the contribution of the target beam. The edges of the focusing spot would cut the speckle elements, and thus the overlapping area A_{pq} that each speckle has inside the focusing spot should also be calculated. Since the reference beam is relatively stationary during scanning, its contribution can be simulated as the expectation values of variables I_{Tp} and φ_{Tp} [26]. Therefore, the resultant phase of the target and reference beams can be determined by Eq. (15).

2.3. Single-point noise

First, we concern about speckle noise with a single-point measurement. The vibration at a single-point can cause bending, stretching and twisting deformations of the vibrating structure. These cause relative motion between the laser and the target surface even if the laser is stationary. If the vibration is periodical, the focusing spot will move with the vibration period (the yellow arrows in Fig. 2 show an example). For the time-neighboring samples in a signal, the displacement $\Delta\vec{x}$ of the focusing spot in a time increment is equal to the vibration velocity $\vec{v}$

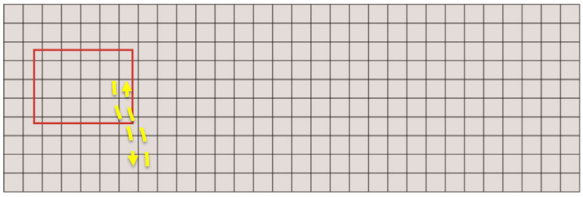

Fig. 2. Example schematic of generating single-point noise. The focusing spot (red rectangle) moves with the vibration period.

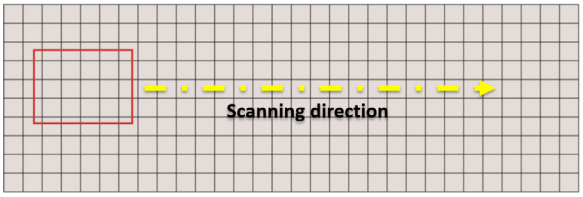

Fig. 3. Example scheme of scanning the vibration surface. The focusing spot (red rectangle) moves along the scanning direction.

divided by the sampling frequency f_s.

$$\Delta\vec{x} = \frac{\vec{v}}{f_s} \tag{17}$$

Then the algorithm for simulating the single-point speckle noise is proposed as Algorithm 1.

Algorithm 1: Simulation of the single-point speckle noise.

Input: the surface roughness parameters, the surface size, the vibration of the focusing node, and the sampling frequency;
1. Divide the surface into $e \times f$ speckle elements, and locate the initial focusing spot;
2. Assign the intensities and phases to the speckle elements according to Equations (10) & (11);
3. Calculate the resultant phase according to Equation (15), and move the focusing spot according to Equation (17) to acquire the time series of $tan(\varphi_{\text{res}})$;
4. Calculate the speckle noise according to Equation (16);
Output: the time series of speckle noise.

2.4. Continuously scanning speckle noise

Second, we are concerned about the measurement strategy of capturing the instantaneous vibrations by continuous scanning. When an LDVom continuously scans the target surface, the focusing spot moves along the scanning direction (in Fig. 3), and the variation inside the photodetector produces the scanning speckle noise. The scanning speed (SS) v_s and the sampling frequency (SF) f_s are two significant factors for simulating speckle noise, as they determine the moving rates of the focusing spot. If the SS-to-SF ratio (SFR) is large, the time-neighboring sampled positions will depart from each other with no overlapping speckle patterns, which results in sharp speckle noise. Otherwise, the noise amplitudes become relatively small.

During the scanning period, the displacement of the focusing spot between two time-neighboring sampled positions can be expressed as

$$\Delta\vec{x} = SFR = \frac{\vec{v}_s}{f_s} \tag{18}$$

Since the target laser focuses the area α speckles $\times$ β speckles at a time instant, the number of overlapped speckle patterns between time-neighboring sampled positions is calculated as follows:

$$N_{\text{overlap}} = \begin{cases} \beta(\alpha - \frac{\Delta x}{d}) = \beta(\alpha - \frac{v_s}{df_s}), & \alpha > \frac{v_s}{df_s} \\ 0, & \alpha \le \frac{v_s}{df_s} \end{cases} \tag{19}$$

where d is the length of a speckle pattern. With the increase in N_{overlap}, the difference between neighboring positions decreases, and thus the speckle noise attenuates. The algorithm for simulating the scanning speckle noise is proposed as Algorithm 2.

Algorithm 2: Simulation of continuously scanning speckle noise.

Input: the surface roughness parameters, the surface size, the scanning speed, and the sampling frequency;
1. Divide the surface into $e \times f$ speckle elements, and locate the initial focusing spot;
2. Assign the intensities and phases to the speckle elements according to Equations (10) & (11);
3. Calculate the resultant phase according to Equation (15), and move the focusing spot along the scanning direction according to Equation (18) to acquire the time series of $tan(\varphi_{\text{res}})$;
4. Calculate the speckle noise according to Equation (16);
Output: the time series of speckle noise.

3. Simulation results

In this section, we demonstrate the validity of the simulation approach by comparing with physical experiments. In order to evalu-

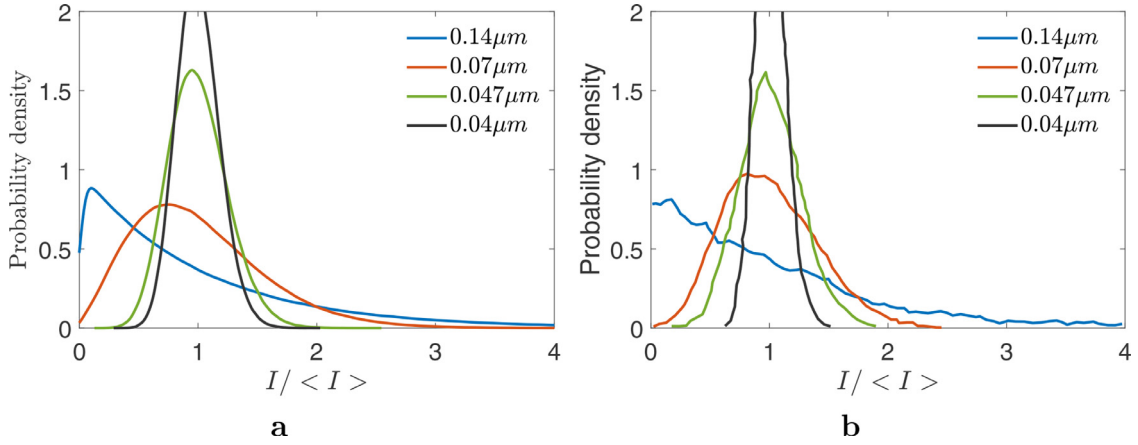

Fig. 4. (**a**) The simulated probability density function of $I/\langle I\rangle$; (**b**) The experimental results reproduced from Ohtsubo and Asakura [20]. The laser wavelength is 0.6328 μm.

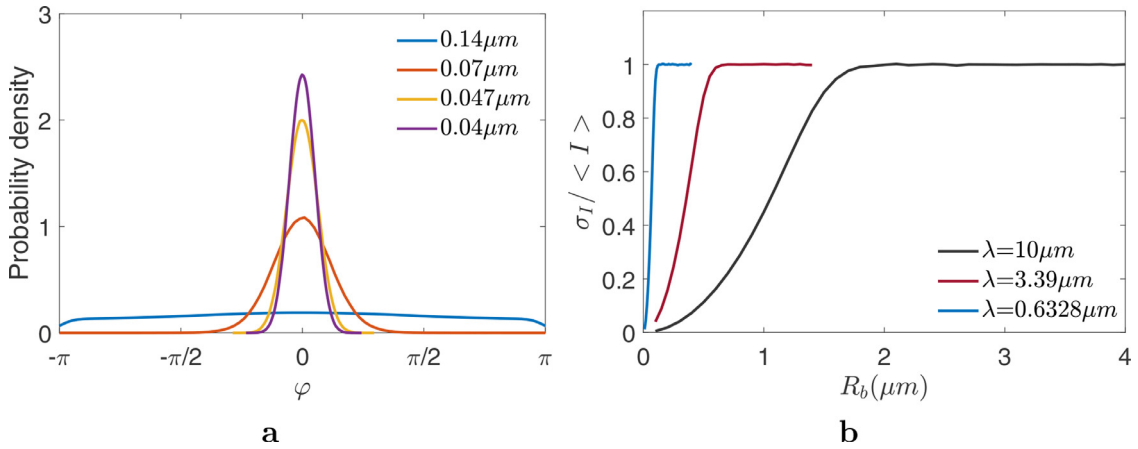

Fig. 5. (**a**) The simulated probability density function of φ (with laser wavelength of 0.6328 μm); (**b**) The relationship between the speckle contrast and surface roughness.

ate our derivation of statistical properties, the phasor distributions of speckle patterns are compared with the experimental work in Ohtsubo and Asakura [20]. Then, to evaluate the simulation of speckle noise, the time series, fast Fourier transform (FFT) spectra, and noise amplitude distribution are compared with the experimental results. Generally, the time series and FFT spectra can roughly compare the similarities between simulation and experiments. Due to the periodical property, the FFT spectra of single-point speckle noise can quantify the noise [34]. The twice-FFT curve of scanning speckle noise can show some similarities although it has no known physical meaning. The probability density function of all magnitudes in the noise series is an effective tool to evaluate the simulation results. After evaluating our simulation approach, several properties of speckle noise are investigated.

3.1. Evaluating the statistical properties

The statistical properties of the speckle patterns constitute the foundation of numerical simulations, thereby requiring appropriate evaluations of the derived distributions. The experimental work in Ohtsubo and Asakura [20] revealed the distribution of the intensity I for rough surfaces (with $R_q = 0.14$, 0.07, 0.047, 0.04 μm) illuminated by the He-Ne laser (with wavelength 0.6328 μm). These parameters are utilized in our simulation to acquire comparison results. Since the microscopic structure of the rough surface is unprovided, a Gaussian distribution is adopted to generate h_k randomly. The probability density function of $I/\langle I\rangle$ ($\langle I\rangle$ is the mean of I) is illustrated in Fig. 4. Our simulated results demonstrate good agreement with the experimental results in Ohtsubo and Asakura [20]. With the decrease in the surface roughness, the probability curves vary from a negative exponential distribution (which agrees with Goodman's results [19]) to a Gaussian distribution centered at $I/\langle I\rangle = 1$. These results indicate the accuracy of simulating the statistical properties.

To investigate the relationship between phase φ and the surface roughness, the probability density function of φ is presented in Fig. 5a. The phase curves are symmetric by 0. When the surface is sufficiently smooth, the speckle phases mostly appear at 0, which indicates that the specular laser wavelets vary little from the incident light. With increasing surface roughness, the phase φ becomes uniformly distributed, agreeing with Goodman's results [19]. Considering the effect of laser wavelength, the relationship between the speckle contrast $\sigma_I/\langle I\rangle$ and surface roughness R_q is shown in Fig. 5b. With a smooth surface, the speckle pattern is almost bright and thus the contrast $\sigma_I/\langle I\rangle$ is nearly 0. With the increasing surface roughness, the speckle pattern becomes dark and bright, and thus its contrast increases. This increasing trend ends at a critical value R_{qc} of the surface roughness. These curves agree with the results in Mansour et al. [18], Fujii and Asakura [21]. The critical value R_{qc} is positively correlated to the incident wavelength since the wavelength determines the laser resolution to the surface roughness.

3.2. Experimental setup

Physical experiments are conducted in the laboratory to evaluate the simulation results. Fig. 6 presents the experimental setup that measures a cantilever strip of length 540 mm. The LDV transmits a laser beam deflected by a rotating mirror to the target surface. (1) When acquiring the single-point speckle noise, the focused node of the strip slightly vibrates at 500 Hz excited by a shaker. Then the LDV acquires the 500 Hz vibration and the speckle noise. (2) When the mirror rotates, the laser continuously scans the steel strip at a constant speed along the scanning direction (Fig. 6a). The laser beam only scans the sample once, not repeatedly or periodically, which satisfies the basic concept of an LDVom. The scanning speed is adjustable. There are no vibrations of the target, and thus the LDVom acquires pure speckle noise. The sampling frequency is 102,400 Hz.

3.3. Single-point simulation

First, the single-point speckle noise is simulated according to the algorithm in Section 2.3, since sometimes important structural nodes need constant monitoring. The frequency of the single-point vibration is simulated as 512 Hz. The simulated frequency of 512 Hz has a small difference from the experimental frequency of 500 Hz, to identify whether the speckle noise is vibration-related. In [34], the peak intervals in the FFT spectra of speckle noise are equaling to motion frequency. We also want to evaluate if the peak intervals change with the vibration frequency. The simulated focusing spot is set 700×700 μm^2 and the laser wavelength is 1.55 μm. These parameters are the same as the LDV. The size of the speckle element is 5×5 μm^2, and the sampling frequency is 102,400 Hz.

Fig. 7 presents the time series of the numerically simulated (with $R_a = 0$ and $R_q = 0.47$μm) and experimentally acquired speckle noise (the single-point vibrations have been removed by subtracting from the LDV signals the vibration input), as well as the FFT spectra. The simulated series of speckle noise presents cyclical fluctuations arising from the 512 Hz vibration, and thus the noise period is 1/512 s. The experimental noise also presents a period of 0.002 s due to the 500 Hz vibration. A good agreement is visible in the FFT spectra. The intervals between frequency spikes in the simulated spectrum are constant (512 Hz), and

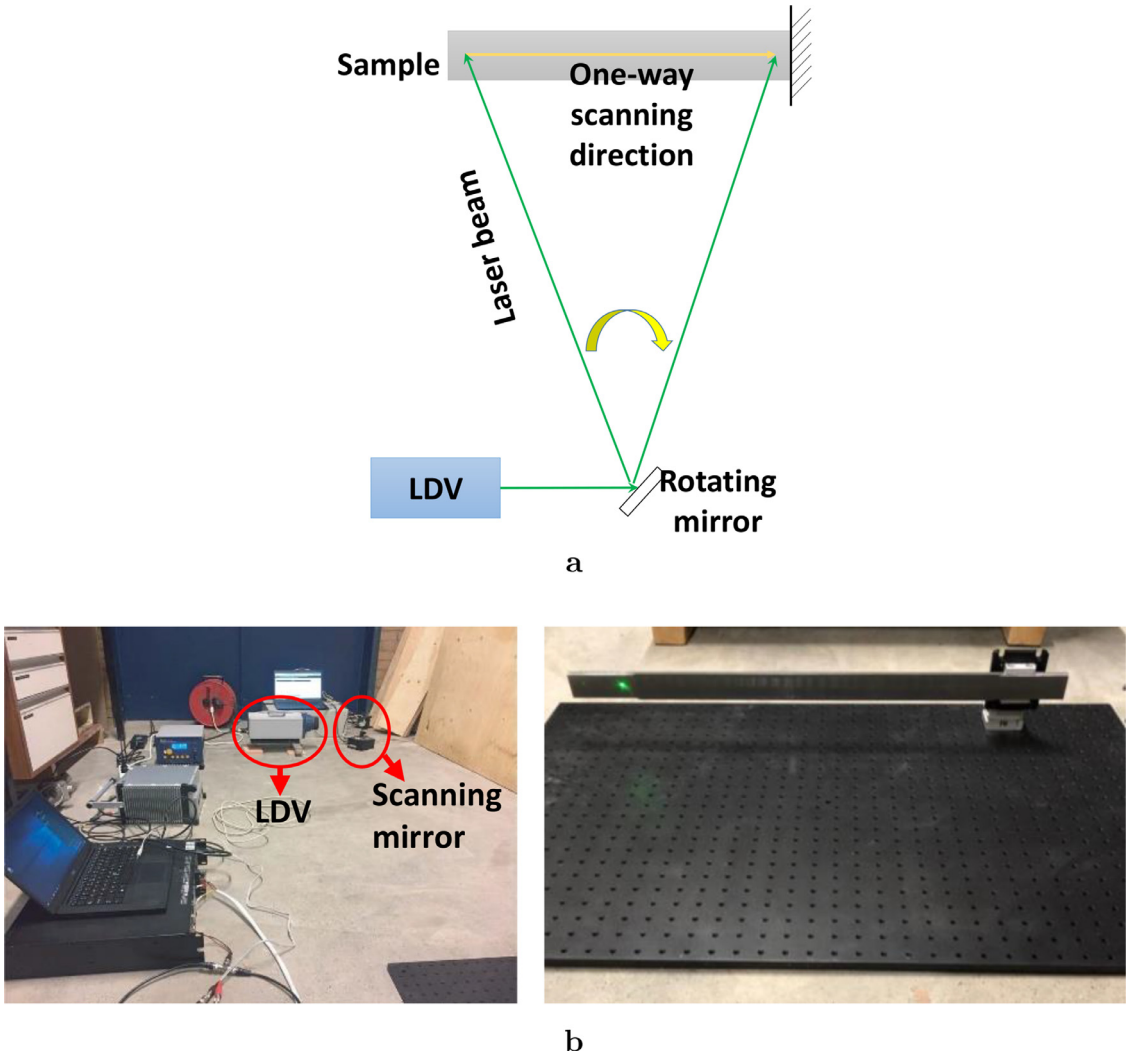

Fig. 6. (**a**) Scheme of the physical experiments; (**b**) experimental set-up for acquiring speckle noise.

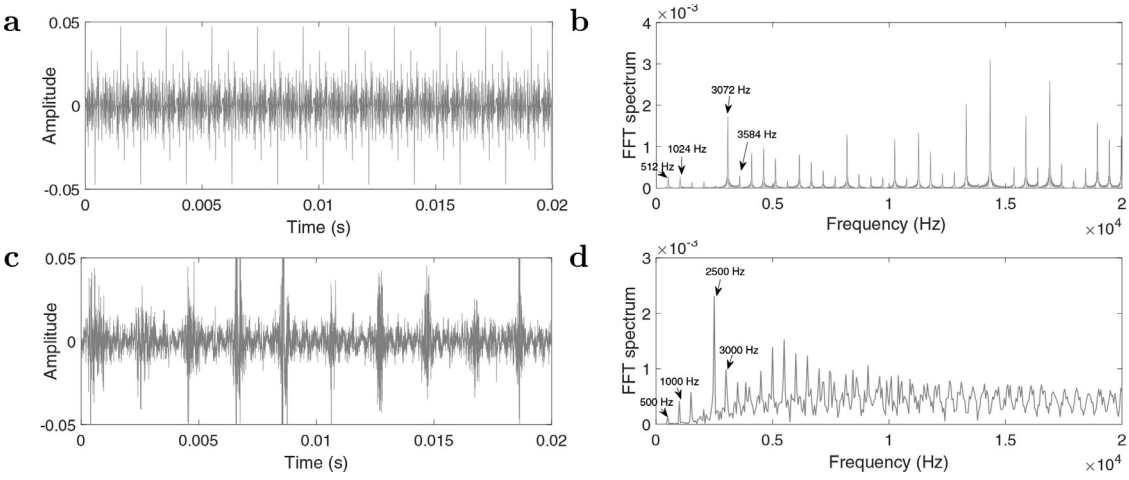

Fig. 7. (**a**) The simulated speckle noise with $R_a = 0$ and $R_q = 0.47\mu m$; (**b**) The FFT spectrum of **a**; (**c**) The experimental speckle noise; (**d**) The FFT spectrum of **c**.

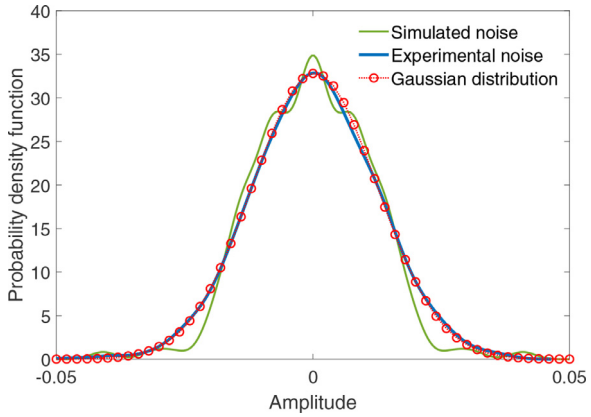

Fig. 8. The probability density function of simulated and experimental noise, as well as a Gaussian distribution.

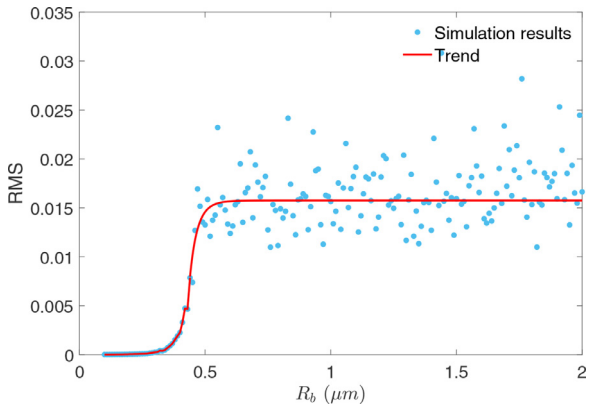

Fig. 9. The relationship between the surface roughness R_q and RMS of the noise amplitude.

those in the experimental spectrum are also constant (500 Hz). Actually, these intervals equal the frequency of the spot motion [34] and thus equal the vibration frequency in this scenario. These well-agreed results demonstrate that the proposed approach is effective in simulating single-point speckle noise. However, the true vibration mixed with the speckle noise at the vibration frequency (512 Hz in the simulation and 500 Hz in the experiment). Although a bandpass filter is effective to remove other harmonics, the vibration energy would be enlarged or underestimated.

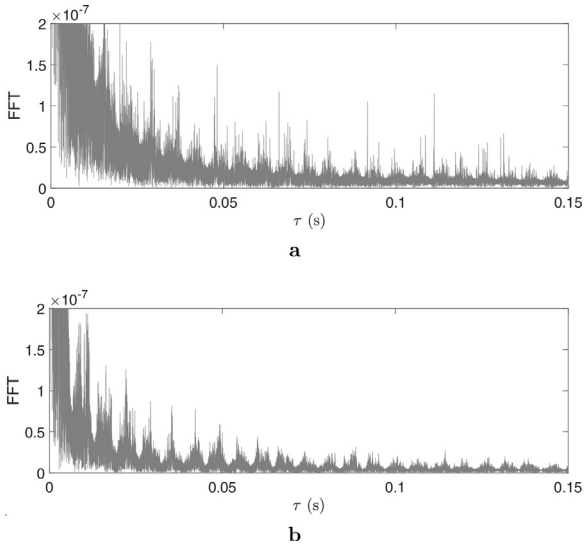

Fig. 11. FFT on the (**a**) simulated frequency spectrum; (**b**) experimental frequency spectrum.

Fig. 8 illustrates the probability density function (PDF) of the noise amplitude, as well as a Gaussian distribution. The simulated noise presents a similar distribution to the experimental noise, which indicates the accuracy of our simulation. The speckle noise amplitude approximately obeys a Gaussian distribution. However, the speckle noise is different from Gaussian white noise since the power spectrum is not uniformly distributed (Fig. 7).

Fig. 9 presents the relationship between the surface roughness R_q and the root-mean-square (RMS) of the noise amplitude. The noise energy increases with the surface roughness when $R_q \leq R'_{qc}$, and fluctuates around a constant when $R_q > R'_{qc}$ (the critical value R'_{bc} is related to the laser wavelength). The increasing noise energy is related to the increasing variance of phase (e.g., Fig. 5a). Therefore, reducing the surface roughness (e.g., by polishing the surface) in small-scale measurement will significantly mitigate speckle noise.

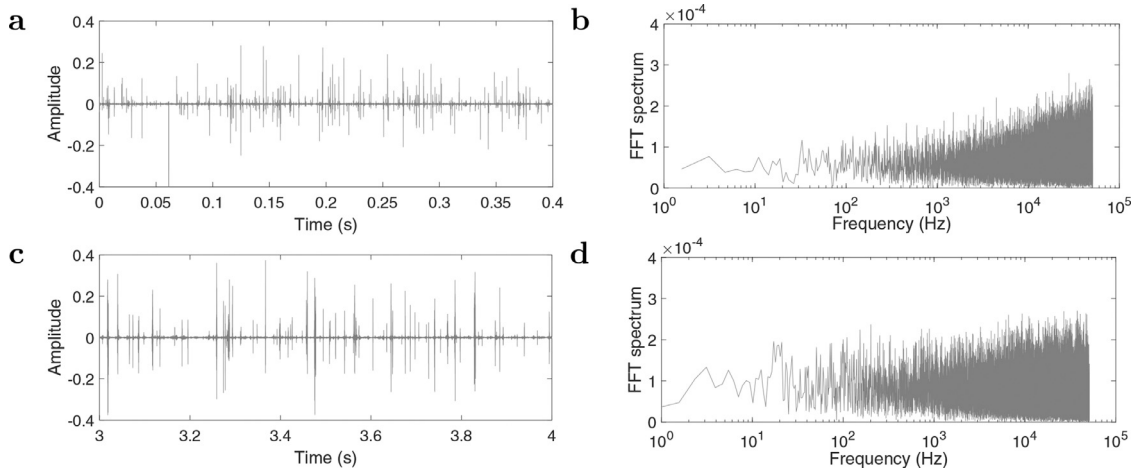

Fig. 10. (**a**) Simulated scanning speckle noise with $R_a = 0$ and $R_q = 0.47\mu$m; (**b**) FFT spectrum of **a;** **c**) Experimental speckle noise (zoom-in between 3 s and 4 s); (**d**) FFT spectrum of **c**. The scanning speed is $v_s = 0.1$ m/s.

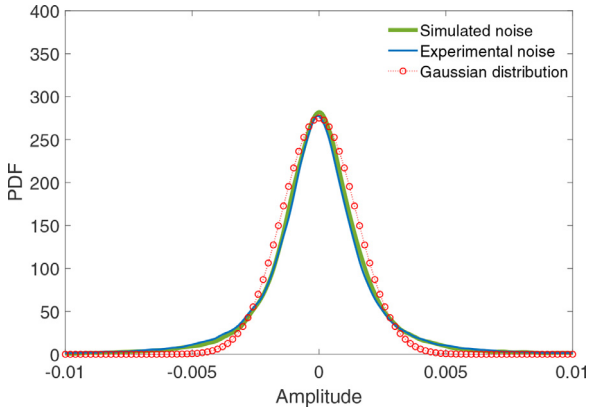

Fig. 12. The probability density function of simulated and experimental scanning noise, as well as Gaussian distribution.

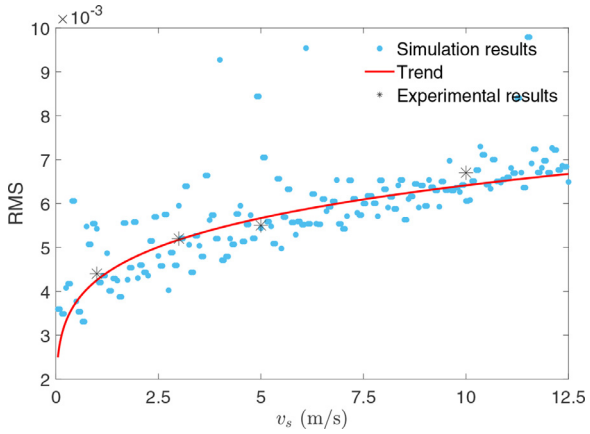

Fig. 14. The relationship between the scanning speed v_s and RMS of the noise amplitude.

3.4. Continuously scanning simulation

Second, we simulate the LDVom speckle noise in continuous scanning, utilizing the algorithm in Section 2.4. The simulation parameters are the same as those in Section 3.3. The scanning surface is 40×540 mm^2 divided into $8000 \times 108{,}000$ rectangle elements. The sampling frequency is 102,400 Hz.

Fig. 10 shows the time series as well as the FFT spectra of both numerically simulated (with $R_a = 0$ and $R_q = 0.47\mu$m) and experimentally acquired speckle noise. The scanning speed is $v_s = 0.1$ m/s. The speckle noise appears in two forms Rothberg et al. [1], the signal drop-outs with extremely large magnitudes and the normal dominant noise with small magnitudes. For both time series, the dominant noise energy is within magnitudes $\lesssim 0.005$, and the signal drop-outs with large magnitudes occasionally appear. Good agreement is achieved between the FFT spectra, as the noise energy increases in the frequency domain and both spectrum curves present similar fluctuations. Different from the FFT spectra of the single-point noise, the intervals between the spikes are nonconstant since the scanning is not cyclical.

To further visualize the simulation accuracy, we conduct FFT on the frequency spectrum in Fig. 10, with the results presented in Fig. 11. The curves decrease exponentially with the increasing τ. The intervals between curve peaks are constant, 6.81×10^{-3} s and 6.78×10^{-3} s for the simulated and experimental results, respectively. These results present good agreement and thus demonstrate the accuracy of our simulation.

The PDF of the noise amplitude and a Gaussian distribution are illustrated in Fig. 12. The PDF curves of the simulated and experimental noise are almost identical. The scanning noise approximately obeys a Gaussian distribution, similar to the single-point noise. However, the speckle noise is different from Gaussian white noise since the power spectrum is not uniformly distributed.

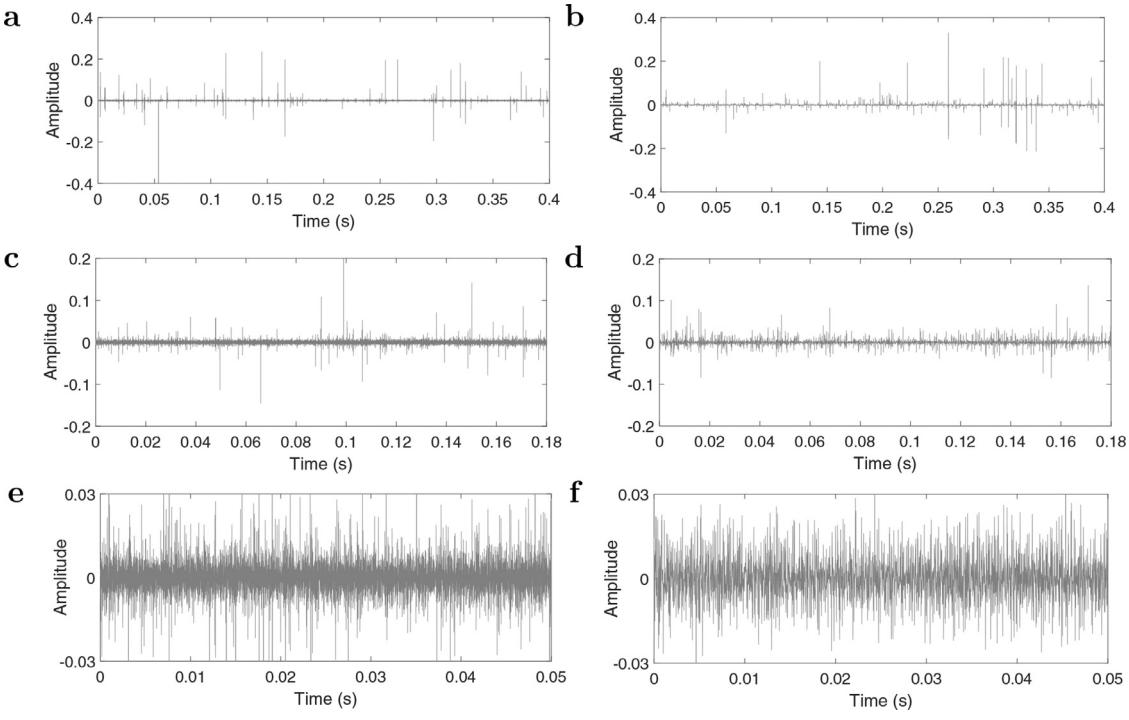

Fig. 13. (**a**) Simulated scanning speckle noise with $v_s = 1$ m/s; (**b**) Experimental scanning speckle noise with $v_s = 1$ m/s; (**c**) Simulated scanning speckle noise with $v_s = 3$ m/s; (**d**) Experimental scanning speckle noise with $v_s = 3$ m/s; (**e**) Simulated scanning speckle noise with $v_s = 10$ m/s; (**f**) Experimental scanning speckle noise with $v_s = 10$ m/s.

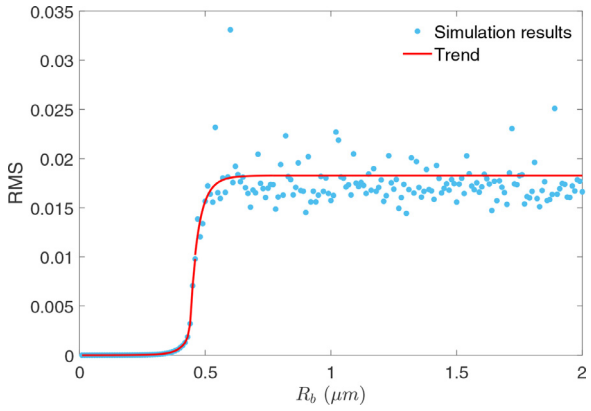

Fig. 15. The relationship between the surface roughness R_q and RMS of the scanning noise amplitude.

To investigate the effect of the scanning speed, we assign the parameters $v_s = 1, 3, 10$ m/s ($f_s = 102,400$ Hz, $R_a = 0$ and $R_q = 0.47\mu$m) in both numerical simulations and experiments, with the speckle noise shown in Fig. 13. The simulated noise presents good agreement with the experimental results. The dominant noise magnitudes increase with increasing scanning speed, but the signal drop-outs decrease in intensity and density. The magnitudes of the signal drop-outs become smaller and the signal drop-outs appear less frequently. This result is also visible in the RMS curve illustrated in Fig. 14, as the simulated noise energy presents an increasing trend despite fluctuations. Therefore, reducing the scanning speed can effectively mitigate the speckle-noise energy.

Further simulations are intended to investigate the relationship between the noise amplitude RMS and the surface roughness, as shown in Fig. 15. Similar to the single-point noise, the scanning noise energy increases with the surface roughness when $R_q \leq R'_{qc}$, and fluctuates around a constant when $R_q > R'_{qc}$. Therefore when additional operations on the scanning surface are convenient, reducing the surface roughness, such as polishing the surface, is an effective strategy to mitigate speckle noise.

4. Discussion

In this paper, we use a commercial LDV from Polytec (model No. RSV-150) to conduct the experiments. It could be a significant issue of our noise analysis if the demodulation system of RSV-150 alters the original signal. Therefore, we discuss some evidences regarding the outputs of the RSV-150 LDV.

Firstly, the LDV header acquires the modulation frequency according to equation (12). The polytec system uses an acousto-optic modulator to shift the laser frequency by a carrier frequency of 40 MHz (add 40 MHz to the modulation frequency), in order to distinguish between movements away from and towards the detector [35,36]. The demodulator is a PM or FM demodulator which is necessary for any LDV to acquire the Doppler frequency shift [37]. The carrier frequency and the demodulator are required for any general LDV, not only the polytec system, and these two components cannot alter the output of the Doppler frequency shift [38]. Therefore, the speckle noise output from RSV-150 is original according to Eq. (13).

Secondly, the promising consistence between our theoretical and experimental results indicate that the speckle noise output from RSV-150 is original. In both single-point and continuously scanning results, the numerically simulated and experimentally acquired speckle noise presents similar amplitude distributions, FFT spectra and energy trends. The agreement indicates that RSV-150 does not alter the original signal.

5. Conclusion

In this paper, we propose a novel approach for numerically simulating the speckle noise in LDVom signals, and then characterize this noise for a better understanding of the signal issue. Single-point speckle noise is also characterized since sometimes important structural nodes need constant monitoring. When investigating the statistical properties, we thoroughly consider the related factors, including the surface roughness. The complex distribution of the speckle phases is then derived. The distributions of the speckle intensity and phase agree well with the experimental results in the literature. These promising statistical properties constitute the foundation of simulating speckle noise.

The single-point and continuously scanning speckle noise are both numerically simulated and experimentally acquired, and their corresponding time-series and FFT spectra present good agreement. For the single-point speckle noise, the intervals of frequency peaks in the FFT spectra are constant and equal to the vibration frequency. The cyclical motion of the laser spot arises from the vibration, and thus the speckle noise presents the same period as the vibration. The simulated noise amplitude presents a similar distribution to the experimental result, approximating a Gaussian distribution. The noise energy increases with the surface roughness when $R_q \leq R_{qc}$, and fluctuates around a constant when $R_q > R_{qc}$. These amplitude and energy properties are also visible for continuously scanning speckle noise. In addition, the energy of the continuously scanning speckle noise increases with the scanning speed, but the signal drop-outs decrease in intensity and density. These results demonstrate the simulation accuracy, and the characteristics of the speckle noise can contribute to future research concerning despeckling procedures or noise avoidance.

Some strategies for mitigating speckle noise are supported by noise characteristics and should be investigated in future research:

i. For single-point speckle noise, the frequency spectra present harmonics that are multiples of the vibration frequency. Therefore, the true vibration is mixed with the speckle noise at the vibration frequency. Although a bandpass filter is effective in removing other harmonics, the vibration energy would be enlarged or underestimated;
ii. During continuously scanning, the noise energy increases with the scanning speed. Therefore, reducing the scanning speed can effectively mitigate speckle noise;
iii. The speckle noise energy increases with surface roughness; thus, reducing the surface roughness, such as polishing the surface, is an effective strategy to mitigate speckle noise. However, it is effective in experimental investigation but not in field measurement.

Declaration of Competing Interest

The authors declare that they have no known competing financial interests or personal relationships that could have appeared to influence the work reported in this paper.

References

[1] Rothberg S, Allen M, Castellini P, Di Maio D, Dirckx J, Ewins D, et al. An international review of laser Doppler vibrometry: making light work of vibration measurement. Opt Lasers Eng 2017;99:11–22.
[2] Nassif HH, Gindy M, Davis J. Comparison of laser Doppler vibrometer with contact sensors for monitoring bridge deflection and vibration. NDTE Int 2005;38(3):213–18.
[3] Sels S, Ribbens B, Bogaerts B, Peeters J, Vanlanduit S. 3D model assisted fully automated scanning laser Doppler vibrometer measurements. Opt Lasers Eng 2017;99:23–30.
[4] Xu Y, Chen D-M, Zhu W. Damage identification of beam structures using free response shapes obtained by use of a continuously scanning laser Dopplervibrometer system. Mech Syst Signal Process 2017;92:226–47.
[5] Allen MS, Sracic MW. A new method for processing impact excited continuous-scan laser Doppler vibrometer measurements. Mech Syst Signal Process 2010;24(3):721–35.
[6] Chen D-M, Xu Y, Zhu W. Identification of damage in plates using full-field measurement with a continuously scanning laser Doppler vibrometer system. J Sound Vib 2018;422:542–67.

[7] Rahimi S, Li Z, Dollevoet R. Measuring with laser Doppler vibrometer on moving frame (ldvmf). In: AIP conference proceedings, vol. 1600. American Institute of Physics; 2014. p. 274–86.
[8] Rothberg S, Baker J, Halliwell N. Laser vibrometry: pseudo-vibrations. J Sound Vib 1989;135(3):516–22.
[9] Martin P, Rothberg S. Introducing speckle noise maps for laser vibrometry. Opt Lasers Eng 2009;47(3–4):431–42.
[10] Jin Y, Li Z. Eliminating speckle noises for laser Dopplervibrometer based on empirical wavelet transform. In: 2021 13th international conference on measurement. IEEE; 2021. p. 72–5.
[11] Vass J, Šmíd R, Randall R, Sovka P, Cristalli C, Torcianti B. Avoidance of speckle noise in laser vibrometry by the use of kurtosis ratio: application to mechanical fault diagnostics. Mech Syst Signal Process 2008;22(3):647–71.
[12] Hosek P. Algorithm for signal drop-out recognition in ic engine valve kinematics signal measured by laser Doppler vibrometer. Opt Laser Technol 2012;44(4):1101–12.
[13] Chiariotti P, Martarelli M, Revel G. Delamination detection by multi-level wavelet processing of continuous scanning laser Doppler vibrometry data. Opt Lasers Eng 2017;99:66–79.
[14] Pieczonka Ł, Ambroziński Ł, Staszewski WJ, Barnoncel D, Pérès P. Damage detection in composite panels based on mode-converted lamb waves sensed using 3d laser scanning vibrometer. Opt Lasers Eng 2017;99:80–7.
[15] Zhu J, Li Y, Baets R. Mitigation of speckle noise in laser Dopplervibrometry by using a scanning average method. Opt Lett 2019;44(7):1860–3.
[16] Xu Y, Chen D-M, Zhu W. Modal parameter estimation using free response measured by a continuously scanning laser Doppler vibrometer system with application to structural damage identification. J Sound Vib 2020;485:115536.
[17] Goodman JW. Dependence of image speckle contrast on surface roughness. Opt Commun 1975;14(3):324–7.
[18] Mansour N, Abd-Rabou A, Elmahdy A, El-Agmy R, El-Nicklawy M. Dependence of speckle contrast on the light spectral broadening and the roughness root mean square. Optik 2017;133:140–9.
[19] Goodman JW. Statistical properties of laser sparkle patterns. Tech. Rep. Stanford Univ CA Stanford Electronics Labs; 1963.
[20] Ohtsubo J, Asakura T. Statistical properties of speckle patterns produced by coherent light at the image and defocus planes. Optik 1976;45(1):65–72.
[21] Fujii H, Asakura T. Effect of surface roughness on the statistical distribution of image speckle intensity. Opt Commun 1974;11(1):35–8.
[22] Bolter R, Gelautz M, Leberl F. SAR speckle simulation. Int Arch Photogramm Remote Sens 1996;31:20–5.
[23] Perreault C, Auclair-Fortier M-F. Speckle simulation based on B-mode echographic image acquisition model. In: Fourth Canadian conference on computer and robot vision (CRV'07). IEEE; 2007. p. 379–86.
[24] Yamaguchi I. Digital simulation of speckle patterns. In: Speckle 2018: VII international conference on speckle metrology, vol. 10834. International Society for Optics and Photonics; 2018. p. 1083409.
[25] Di Martino G, Iodice A, Riccio D, Ruello G. A physical approach for SAR speckle simulation: first results. Eur J Remote Sens 2013;46(1):823–36.
[26] Rothberg S. Numerical simulation of speckle noise in laser vibrometry. Appl Opt 2006;45(19):4523–33.
[27] Goodman JW. Speckle phenomena in optics: theory and applications. Roberts and Company Publishers; 2007.
[28] Dainty JC. Laser speckle and related phenomena, vol 9. Springer Science & Business Media; 2013.
[29] Pedersen HM. Object-roughness dependence of partially developed speckle patterns in coherent light. Opt Commun 1976;16(1):63–7.
[30] Persson U. Real time measurement of surface roughness on ground surfaces using speckle-contrast technique. Opt Lasers Eng 1992;17(2):61–7.
[31] Erf R. Speckle metrology. Elsevier; 2012.
[32] Cedilnik A, Kosmelj K, Blejec A. The distribution of the ratio of jointly normal variables. Metodol Zvezki 2004;1(1):99.
[33] Halliwell NA. Laser vibrometry. In: Optical methods in engineering metrology. Springer; 1993. p. 179–211.
[34] Martarelli M, Ewins DJ. Continuous scanning laser Doppler vibrometry and speckle noise occurrence. Mech Syst Signal Process 2006;20(8):2277–89.
[35] Laser Doppler vibrometry technology from polytec. Accessed: 2022-04-04 https://www.polytec.com/int/vibrometry/technology/laser-doppler-vibrometry.
[36] Polytec RSV-150. Accessed: 2022-04-04 https://www.polytec.com/int/vibrometry/products/special-application-vibrometers/rsv-150-remote-sensing-vibrometer.
[37] Dräbenstedt A, Sauer J, Rembe C. Remote-sensing vibrometry at 1550 nm wavelength. In: AIP conference proceedings, vol. 1457. American Institute of Physics; 2012. p. 113–21.
[38] Strean R, Mitchell L, Barker A. Global noise characteristics of a laser Dopplervibrometer-I. Theory. Opt Lasers Eng 1998;30(2):127–39.